Thermodynamical properties of a mean-field plus pairing model and applications for the Fe nuclei

S. Rombouts,* K. Heyde,† and N. Jachowicz
Vakgroep Subatomaire en Stralingsfysica, Universiteit Gent, Proeftuinstraat 86, B-9000 Gent, Belgium
(Received 28 April 1998)

A mean-field plus pairing model for atomic nuclei in the Fe region was studied using a finite-temperature quantum Monte Carlo method. We present results for thermodynamical quantities such as the internal energy and the specific heat. These results give indications of a phase transition related to the pairing among nucleons, around temperatures of 0.7 MeV. The influence of the residual interaction and of the size of the model space on the nuclear level densities is discussed too.
[S0556-2813(98)01712-9]

PACS number(s): 21.60.Ka, 21.10.Ma, 21.60.Cs, 27.40.+z

I. INTRODUCTION

Quantum Monte Carlo methods offer an interesting way to study fermionic many-body problems. Accurate calculations of ground-state properties have been performed for light nuclei, using variational and diffusion quantum Monte Carlo methods [1]. Also, for the nuclear shell model, Monte Carlo methods are very useful [2]. They allow one to do calculations in much larger model spaces than conventional techniques based on diagonalization. Furthermore, they are very useful for the study of finite-temperature properties of atomic nuclei [3,4]. The same method can also be used as a starting point to calculate nuclear level densities [5,6]. We have used a variant of this method to study thermodynamical properties of nuclei in the Fe region with a model based on a mean-field plus pairing Hamiltonian. At present, we are limited to this too simple model because our quantum Monte Carlo method is still in a developing phase and because we are limited by our present computer facilities (a Dec Alphastation 255/300 MHz Workstation and a 200 MHz Pentium personal computer). Even though, at present, our results do not conform to realistic Hamiltonians, they do say a lot about the general physical properties. It is a first step to go beyond the mean-field approximation. The present approach gives results about the possibility of a phase transition related to pairing correlations, the influence of the residual interaction on the level densities, and a number of general features of the nuclear many-body structure at finite temperature.

The combination of a mean-field potential and the pairing Hamiltonian leads to a Hamiltonian $\hat{H}=\hat{H}_{\mathrm{mf}}+\hat{H}_P$. Though this Hamiltonian looks simple, it already leads to a complicated many-body problem. An often used technique to tackle this problem is the Bardeen-Cooper-Schrieffer (BCS) theory [7]. It leads to equations that can be handled easily in a numerical way and it has a clear interpretation in terms of quasiparticles. The disadvantage is that it gives only an approximate solution and leads to many-body states in which the number of particles is not fixed. For some systems, exact solutions can be found [8]. A general, accurate solution for this many-body problem is even at present a topic of intensive research [9,10]. We have found that our quantum Monte Carlo method is a very useful method to study the ground-state and finite-temperature properties of the nuclear pairing Hamiltonian.

In Sec. II we introduce the mean-field plus pairing model that we used for our calculations. In Sec. III aspects of our quantum Monte Carlo method are given, with an emphasis on the differences with related methods. In Sec. IV we present a number of results. The role of the pairing-interaction strength, the size of the model space, and the number of particles is discussed. An estimate is given for the level densities. The lines that connect the data points on the figures in this paper are meant to guide the eye. They do not correspond to analytical results or fitted curves, except for the pure mean-field results ($G=0$). Error limits represent 95% confidence intervals. If no error limits are shown, it means that they are smaller than the markers of the data points, unless it is stated that no error limits were determined.

II. A MEAN-FIELD PLUS PAIRING MODEL FOR THE Fe NUCLEI

For the mean-field potential, a Woods-Saxon potential $U(r)$ is used [11]:

$$U(r)=V_c-Vf(x)+\left(\frac{\hbar}{m_\pi c}\right)^2 V_{\mathrm{s.o.}}(\boldsymbol{\sigma}\cdot\mathbf{l})\frac{1}{r}\frac{d}{dr}f(x_{\mathrm{s.o.}}), \quad (1)$$

where

$$V_c=\begin{cases} Ze^2/r, & r\geqslant R_c \\ [Ze^2/2R_c](3-r^2/R_c^2), & r\leqslant R_c, \end{cases} \quad (2)$$

$$R_c=r_cA^{1/3},$$

$$f(x)=(1+e^x)^{-1} \ \text{ with } \ x=(r-r_0A^{1/3})/a, \quad (3)$$

$$\left(\frac{\hbar}{m_\pi c}\right)^2=2.000\ \mathrm{fm}^2. \quad (4)$$

*Electronic address: Stefan.rombouts@rug.ac.be
†Electronic address: Kris.Heyde@rug.ac.be. Present address: EI-Isolde CERN, CH 1211, Geneva 23, Switzerland.

TABLE I. Single-particle eigenstates of the Woods-Saxon potential with the parameters as described in Sec. II.

	Single-particle energies (MeV)	
Orbital	Protons	Neutrons
$1s_{1/2}$	−34.7106	−42.0333
$1p_{3/2}$	−25.3351	−32.2120
$1p_{1/2}$	−24.0715	−31.1979
$1d_{5/2}$	−15.0034	−21.5607
$1d_{3/2}$	−12.7911	−19.6359
$2s_{1/2}$	−12.3511	−19.1840
$1f_{7/2}$	−4.1205	−10.4576
$2p_{3/2}$	−2.0360	−8.4804
$2p_{1/2}$	−1.2334	−7.6512
$1f_{5/2}$	−1.2159	−7.7025
$3s_{1/2}$	4.7316	−0.3861
$2d_{5/2}$	5.6562	0.2225
$2d_{3/2}$	6.1324	0.9907
$1g_{9/2}$	6.6572	0.5631
$3p_{3/2}$	6.6663	2.5931
$3p_{1/2}$	6.7469	2.6915
$4s_{1/2}$	8.9016	4.4706
$1g_{7/2}$	9.1386	3.5488

Here A is the number of nucleons and Z the number of protons. The other parameters are taken as in [12]:

$$r_0 = 1.25 \text{ fm},$$

$$a = 0.65 \text{ fm},$$

$$V = 53.3 + 27(A-2Z)/A - 0.4Z/A^{1/3} \text{ MeV},$$

$$r_{so} = 1.25 \text{ fm},$$

$$a_{so} = 0.47 \text{ fm},$$

$$V_{so} = 7.5 \text{ MeV}.$$

To calculate the mean field and its eigenfunctions, we use the parameters for the nucleus $^{56}_{26}\mathrm{Fe}_{30}$. This mean field is used for all nuclei in this particular mass region. For every set of quantum numbers l and j, the Woods-Saxon potential is diagonalized in a basis of the lowest 60 harmonic-oscillator eigenfunctions with the appropriate symmetry. In this way, the single-particle eigenstates and their energies listed in Table I are obtained. Also, a number of unbound states (with energy $E>0$) are obtained. In fact, the Woods-Saxon potential exhibits a continuum of unbound eigenstates. Due to the expansion in a finite number of basis functions, discrete unbound energy levels are obtained. These can be seen as a discrete approximation to the continuum of unbound states. The $1s_{1/2}$, $1p_{3/2}$, $1p_{1/2}$, $1d_{5/2}$, $1d_{3/2}$, and $2s_{1/2}$ orbitals are considered to be completely filled. They form an inert core for the many-body problem. The $1f_{7/2}$, $2p_{3/2}$, $2p_{1/2}$, and $1f_{5/2}$ orbitals constitute the valence shell.

A simple Hamiltonian that accounts for the short-range correlations induced by the residual interaction is the nuclear pairing Hamiltonian $\hat{H}_P$ [7], which takes the form

$$\hat{H}_P = -\sum_{t=p,n} G_t \sum_{k,k'>0} \hat{a}^\dagger_{k't} \hat{a}^\dagger_{\overline{k}'t} \hat{a}_{\overline{k}t} \hat{a}_{kt}, \tag{5}$$

where the operators $\hat{a}^\dagger_{kt}$ create a particle in the corresponding single-particle eigenstates of the mean-field Hamiltonian in the valence shell. The index t indicates proton or neutron states and $\overline{k}$ is the time-reversed state of the state k. The notation $k,k'>0$ denotes that the summation for k and k' should run over states with angular momentum projection $j_z>0$ only. The interaction strength G_t depends on the model space and the system under study. For the strength of the pairing interaction we take $G=20$ MeV/56, following the suggestion of Bes and Sorensen [13] to take $G=20$ MeV/nucleon. The same strength is used for protons, neutrons, and all nuclei in the Fe mass region.

III. THE QUANTUM MONTE CARLO METHOD

The method we used to study the model is based on the shell-model quantum Monte Carlo method. The basic idea of this method is well explained in Ref. [2]. It amounts to a decomposition of the Boltzmann operator $e^{-\beta\hat{H}}$ in a sum of exponentials of one-body operators

$$e^{-\beta\hat{H}} = \sum_\sigma e^{-\hat{h}_{\beta,\sigma}}. \tag{6}$$

Because of their one-body nature, the terms $e^{-\hat{h}_{\beta,\sigma}}$ can be handled easily using small matrices, with a dimension equal to the number of single-particle states considered in the model space. The canonical or grand canonical trace of $e^{-\hat{h}_{\beta,\sigma}}$ can be calculated with simple algebraic operations on these matrices. The sum over the *auxiliary field* σ is then evaluated using Monte Carlo techniques (*in casu* the Metropolis algorithm [14]).

In our approach, a number of technical aspects are implemented differently from Ref. [2]. The main differences are the following.

(i) In order to arrive at a decomposition of the form (6), we use the Suzuki-Trotter formula [15] to separate the one- and two-body parts of the Hamiltonian in the exponents. This reduces the leading systematic error term to order β^3/N_t^2, with N_t the number of inverse-temperature slices. Following the prescriptions from Ref. [2], the leading systematic error term would be of order β^2/N_t.

(ii) In order to decompose the exponential of the two-body part of the Hamiltonian, we use the discrete Hubbard-Stratonovich transform, described in [16]. Compared to the Hubbard-Stratonovich transform described in [2,17,18], it has the advantage that it leads to faster matrix operations and to smaller systematic errors. Because of these fast matrix operations, we could use a large number of inverse-temperature slices in order to reduce the systematic errors (typically $N_t=20\beta$ for the fp model space and $N_t=40\beta$ for the extended model spaces).

(iii) In order to evaluate the canonical trace of $e^{-\hat{h}_{\beta,\sigma}}$, we use the fast and efficient algorithm described in Ref. [19] instead of the number projection technique described in [2,20].

(iv) The trial steps for the Metropolis algorithm for the sampling of the discrete auxiliary fields σ are generated in the following way. A series of M consecutive inverse $-$temperature intervals are chosen randomly to be updated. Because of the permutation properties of the canonical trace, we can always shift these inverse-temperature intervals to the end of the decomposition. The matrix representation U_σ of the operator $e^{-\beta\hat{h}_\sigma}$ is calculated up to the (N_t-M)th inverse-temperature slice and stored in computer memory. A number m between 1 and a maximum number is drawn. Then in the last M slices m auxiliary fields are drawn. These are then changed randomly. The matrix $U_{\sigma'}$ for the altered configuration σ' is constructed out of the stored part of U_σ. The canonical trace of $U_{\sigma'}$ is evaluated. Then the configuration σ is accepted or rejected according to the Metropolis algorithm [14]. This procedure is repeated a number of times (typically seven times) before a new series of M slices is selected. So a complete Markov step consists of seven local updates. Typical values are $M=80$ (or $M=N_t$ for $N_t<80$) and $1<m<160$. This scheme allows one to update a large number of auxiliary fields simultaneously while requiring only M matrix multiplications per update (counting the contribution of one inverse-temperature slice as one matrix). Only after a complete Markov step do all the N_t matrices in the decomposition have to be multiplied.

(v) Observables are evaluated after every five complete Markov steps. The values are not yet fully decorrelated at this rate (e.g., autocorrelations between 30% and 60% between consecutive values for the energy), leaving a larger interval would not improve the performance because already at this rate the most time-consuming part is the construction of the trial configurations for the Markov chain. The value of an observable $\hat{A}$ at inverse temperature $\beta=1/kT$ is calculated as

$$\langle\hat{A}\rangle_\beta=\frac{\mathrm{Tr}_N(\hat{A}e^{-\beta\hat{H}})}{\mathrm{Tr}_N(e^{-\beta\hat{H}})} \tag{7}$$

$$=\frac{\frac{d}{d\epsilon}\mathrm{Tr}_N(e^{-\beta\hat{H}+\epsilon\hat{A}})\big|_{\epsilon=0}}{\mathrm{Tr}_N(e^{-\beta\hat{H}})} \tag{8}$$

$$=\mathcal{E}_w(A), \tag{9}$$

with

$$\mathcal{E}_w(A)=\frac{\sum_\sigma A_\sigma w_\sigma}{\sum_{\sigma'} w_{\sigma'}}, \tag{10}$$

$$A_\sigma=\frac{d}{d\epsilon}\ln[\mathrm{Tr}_N(e^{\hat{h}_{\beta,\sigma,\epsilon}})]\big|_{\epsilon=0}, \tag{11}$$

$$w_\sigma=\mathrm{Tr}_N(e^{\hat{h}_{\beta,\sigma}}). \tag{12}$$

Here Tr_N denotes the canonical trace, i.e., the trace over all N-particle states. The mathematical properties of the trace operator are crucial in going from expression (7) to expression (8). The one-body operator resulting from the decomposition (6), with $-\beta\hat{H}$ replaced by $-\beta\hat{H}+\epsilon\hat{A}$, is denoted by $\hat{h}_{\beta,\sigma,\epsilon}$. For the energy ($\hat{A}=\hat{H}$), this can easily be implemented as $\hat{h}_{\beta,\sigma,\epsilon}=\hat{h}_{\beta-\epsilon,\sigma}$. The derivatives are evaluated as

$$\frac{d}{d\epsilon}f(\epsilon)\big|_{\epsilon=0}\simeq\frac{f(\epsilon_0)-f(-\epsilon_0)}{2\epsilon_0}, \tag{13}$$

with ϵ_0 a small but finite number (typically $\epsilon_0=1/2048$). This way of evaluating observables requires many matrix manipulations because the complete matrix U_σ has to be recalculated from scratch for $\hat{h}_{\beta,\sigma,\epsilon_0}$ and $\hat{h}_{\beta,\sigma,-\epsilon_0}$. However, because most of the computing time goes to the construction of the trial moves, this has little impact on the overall performance. Furthermore, this way of evaluating the observables leads to small statistical errors because it amounts to an insertion of the operator $\hat{A}$ at each inverse-temperature interval, whereas the procedure described in [2] is based on the insertion of $\hat{A}$ only at the first interval. A special remark concerns the evaluation of the specific heat C. This quantity cannot be calculated as the expectation value of an observable. We evaluate C after the Monte Carlo run as

$$C=\beta^2[\mathcal{E}_w(E_2)-\mathcal{E}_w(E)^2], \tag{14}$$

with

$$E_\sigma=-\frac{d}{d\beta}\ln[\mathrm{Tr}_N(e^{\hat{h}_{\beta,\sigma}})],$$

$$E_{2\sigma}=\frac{d^2}{(d\beta)^2}\ln[\mathrm{Tr}_N(e^{\hat{h}_{\beta,\sigma}})]+E_\sigma^2.$$

The observable E_2 corresponds to the square of the Hamiltonian

$$\mathcal{E}_w(E_2)=\mathrm{Tr}_N(\hat{H}^2e^{-\beta\hat{H}})/\mathrm{Tr}_N(e^{-\beta\hat{H}}). \tag{15}$$

(vi) Just like any other quantum Monte Carlo method for fermions [21,22], this method suffers from a sign problem at low temperatures. The value of the weights w_σ can become negative. This poses a problem for the Metropolis algorithm because it requires that w_σ can be interpreted as a probability density. The Metropolis algorithm can still be used by applying it to the absolute value $|w_\sigma|$. Then we have to treat the sign s_σ of w_σ as an observable. Expression (9) becomes:

$$\langle\hat{A}\rangle_\beta=\frac{\sum_\sigma A_\sigma s_\sigma|w_\sigma|}{\sum_{\sigma'} s_\sigma|w_{\sigma'}|}=\frac{\mathcal{E}_{|w|}(As)}{\mathcal{E}_{|w|}(s)}. \tag{16}$$

The problem is that the statistical error on this expression scales as $1/\mathcal{E}_{|w|}(s)$ (see below). Now, for an even number of protons and an even number of neutrons, one can exploit a symmetry between states with $j_z>0$ and states with $j_z<0$. This symmetry guarantees that $\mathcal{E}_{|w|}(s)$ is close to 1 even at low temperature [16]. In Ref. [2] it was claimed that the

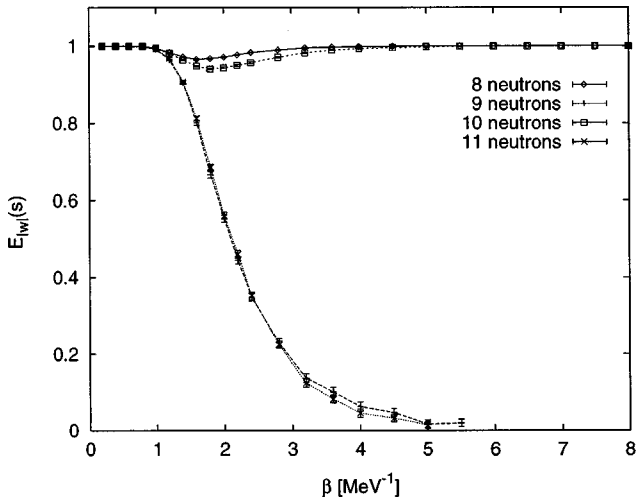

FIG. 1. Average sign $\overline{s}$ as a function of inverse temperature β for 8, 9, 10, and 11 neutrons in the $1f_{7/2}2p_{3/2}2p_{1/2}1f_{5/2}$ shell. $G=20$ MeV/56.

canonical trace should be exactly equal to one for even particle numbers with interactions that lead to matrix representations of the form

$$U_\sigma=\begin{pmatrix} P & Q \\ -Q^* & P^* \end{pmatrix}, \tag{17}$$

as is the case with a pure pairing force or a pairing-plus-quadrupole force. This is not exactly true, however, as can be seen from the following counterexample. Let U_σ be a 4×4 matrix and P and Q 2×2 matrices, with $Q=0$ and

$$P=\begin{pmatrix} \epsilon & 0 \\ 0 & -\epsilon \end{pmatrix}, \tag{18}$$

where ϵ is a real number. Then the grand canonical trace is given by

$$\mathrm{Tr}_\mu(\hat{U}_\sigma)=(1-\epsilon^2e^{2\beta\mu})^2=1-2\epsilon^2e^{2\beta\mu}+\epsilon^4e^{4\beta\mu}, \tag{19}$$

which is positive definite for any value of the chemical potential μ. The canonical two-particle trace is given by the coefficient of $e^{2\beta\mu}$:

$$\mathrm{Tr}_2(\hat{U}_\sigma)=-2\epsilon^2, \tag{20}$$

which is negative. The average sign for some of the systems we studied is shown in Fig. 1 as a function of the inverse temperature β. The sign for the even particle numbers shows a dip around $\beta=2$ MeV^{-1}. This is caused by the fact that for a fraction of the U_σ the canonical trace becomes negative, like in the above example. However, the symmetry between $j_z>0$ states and $j_z<0$ states guarantees that the contribution to the trace of the ''fully accompanied'' states, in the sense defined in Ref. [9], will always be positive. These states dominate the low temperature trace for even-even nuclei. Therefore, the sign tends to one again at low temperatures. For odd particle numbers, $\mathcal{E}_{|w|}(s)$ tends to zero at low temperatures. So there the statistical errors explode. We find that even for odd nuclei we can do calculations at $\beta=4$ MeV^{-1}, which is enough to cool the system almost completely to its ground state. For the model studied here, the average sign posed no problems. However, for more complicated Hamiltonians, one probably will have to fall back on extrapolation techniques such as the ones described in Refs. [2] and [23] in order to overcome the sign problem.

(vii) Because the Metropolis algorithm leads to correlations among successive values for the observables, care has to be taken to establish accurate error limits. In order to get rid of the correlations, 50 independent Markov chains are run for each calculation. These Markov chains typically consist of some 600 thermalization steps and 3000 sampling steps, with an evaluation of observables every fifth step. So the chains are rather short, but long enough to make sure that the computing time is not dominated by the thermalization steps. This leads to 50 independent estimates $A_1,\ldots,A_{50}$ for the quantity $\langle\hat{A}\rangle_\beta$. To obtain the final estimate, we take the weighted average of these values, with the average signs $s_1,\ldots,s_{50}$ as weights. So we obtain an estimate $\overline{A}$ for $\langle\hat{A}\rangle_\beta$:

$$\overline{A}=\frac{\Sigma_i A_i s_i}{\Sigma_j s_j}. \tag{21}$$

If the A_i and s_i are obtained with enough precision, then a good estimate for the statistical error on 21 can be obtained from the expression [24]

$$\mathrm{var}(x/y)=\{\mathrm{var}(x)-2\mathcal{E}(x/y)\mathrm{cov}(x,y)+\mathcal{E}^2(x/y)\mathrm{var}(y)\}/\mathcal{E}^2(y) \tag{22}$$

(var and cov denote the variance and covariance). Taking $x=As$ and $y=s$ leads to an estimate for the variance on $\overline{A}$

$$\mathrm{var}(\overline{A})\simeq\frac{\Sigma_i(A_i-\overline{A})^2s_i^2}{\left(\Sigma_j s_j\right)^2}. \tag{23}$$

Under the assumption that $\overline{A}$ is almost normally distributed, which is a good approximation because $\overline{A}$ is a weighted average of 50 independent values, this expression allows us to determine a 95% confidence interval $[\overline{A}-2\sqrt{\mathrm{var}(\overline{A})},\overline{A}+2\sqrt{\mathrm{var}(\overline{A})}]$ for $\langle\hat{A}\rangle_\beta$. Expression (23) also demonstrates that the statistical error is inversely proportional to the average sign $\mathcal{E}_{|w|}(s)$.

IV. RESULTS

A. Proton and neutron contributions

Some thermodynamical properties of the pairing model for $^{56}_{26}\mathrm{Fe}_{30}$were studied using the quantum Monte Carlo method presented in Sec. III. Because the proton and neutron systems are not coupled to one another, separate results for both particle types are obtained. The internal energy of the total system and the contributions of the proton and neutron subsystems are shown as a function of temperature in Fig. 2. The same is done for the specific heat in Fig. 3. The neutrons contribute more to the internal energy than the protons do because there are more valence neutrons than valence protons. This also leads to a slightly stronger peak in the specific-heat curve for neutrons than for protons. Qualita-

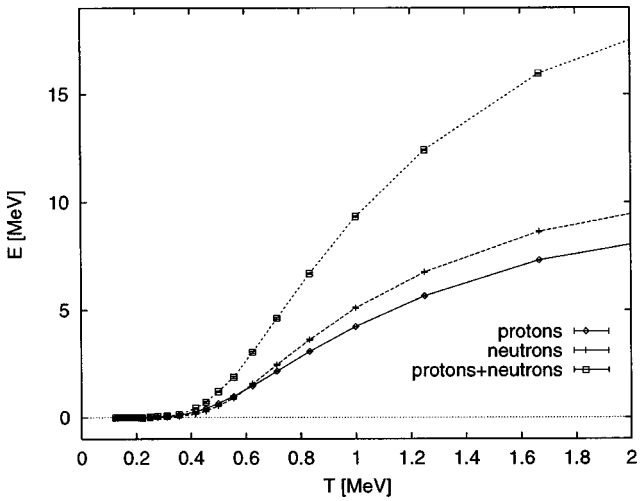

FIG. 2. Internal energy E as a function of temperature T for 6 protons and 10 neutrons in the $1f_{7/1}2p_{3/2}2p_{1/2}1f_{5/2}$ shell. $G=20$ MeV/56. The energy scale is adapted such that the total, proton, and neutron internal energies all tend to 0 at low temperature.

tively, there is no big difference between the thermodynamical properties of both subsystems. This is not the case at lower values of the interaction strength G.

B. Dependence on the pairing interaction strength G

We have studied the pairing model for $^{56}_{26}Fe_{30}$ for several values of the pairing interaction strength. Calculations were performed for 10 neutrons in a shell with 20 valence states ($1f_{7/2}$, $2p_{3/2}$, $2p_{1/2}$ and $1f_{5/2}$ orbitals) and for 6 protons in the same shell.

The neutron energy as a function of temperature is shown in Fig. 4. The energy scale is chosen such that the inert core has zero energy. The fact that the energy does not go to much higher values as the temperature increases is due to the limited size of the model space: Not enough high-lying states are included. As we shall discuss later on, the results for $T \geqslant 1.5$ MeV are not physical any longer. For larger values of G, the system is more strongly bound. Furthermore, when

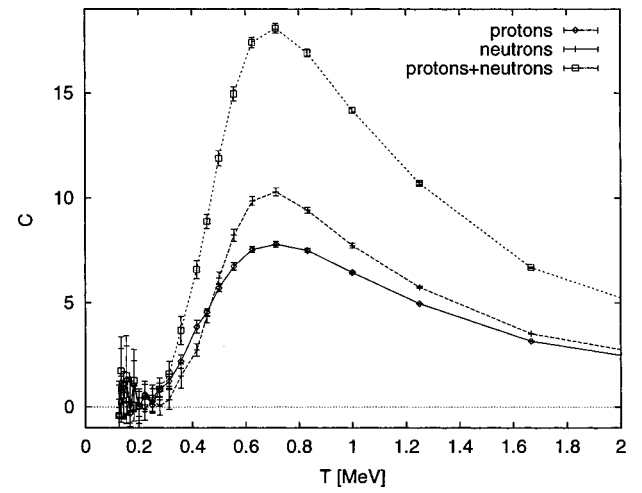

FIG. 3. Specific heat C as a function of temperature T for 6 protons and 10 neutrons in the $1f_{7/2}2p_{3/2}2p_{1/2}1f_{5/2}$ shell. $G=20$ MeV/56.

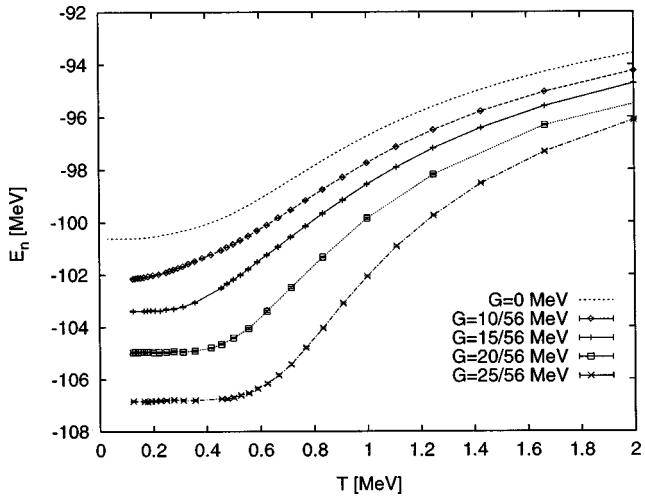

FIG. 4. Neutron energy E_n as a function of temperature T for 10 neutrons in the $1f_{7/2}2p_{3/2}2p_{1/2}1f_{5/2}$ shell for various values of the pairing strength G.

raising the temperature, the system stays in its ground state longer than for smaller values of G. This indicates that there is an energy gap between the ground state and the first excited state proportional to G, as is expected from BCS theory [7]. The neutron specific heat, as a function of temperature, is shown in Fig. 5. With increasing strength G, the peak in the specific-heat curve shifts to a slightly higher temperature and becomes more pronounced. In general, peaks in the specific heat can be interpreted as signs of a phase transition. We see here that the pairing correlations, for $G \geqslant 20$ MeV/56, seem to induce a phase transition in the system.

Analogous calculations were done for protons. The proton energy as a function of temperature is shown in Fig. 6. The proton specific heat is shown as a function of temperature in Fig. 7. The same discussion as for the neutron results applies here. There is, however, a striking difference in the specific-heat curve for low values of G: A second peak develops around $T=0.2$ MeV for $G=10$ MeV/56. At this value of

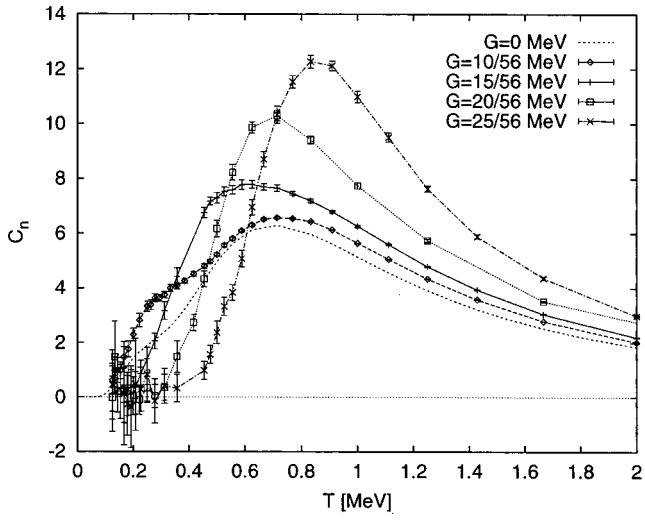

FIG. 5. Neutron specific heat C_n as a function of temperature T for 10 neutrons in the $1f_{7/2}2p_{3/2}2p_{1/2}1f_{5/2}$ shell for various values of the pairing strength G.

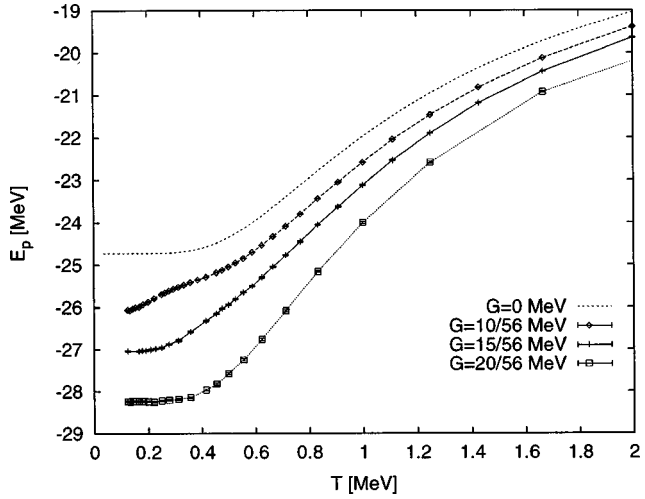

FIG. 6. Proton energy E_p as a function of temperature T for 6 protons in the $1f_{7/2}2p_{3/2}2p_{1/2}1f_{5/2}$ shell for various values of the pairing strength G.

the pairing strength, the broad peak in the specific-heat curve, around $T=0.8$ MeV, coincides with the peak in the specific-heat curve for a pure mean field. This peak is related to the condensation of the valence particles in the lowest-energy levels of the valence shell (the $1f_{7/2}$ orbital). The smaller is entirely due to pair correlations that develop among the six particles in the $1f_{7/2}$ orbital. In Fig. 8 the expectation value of the pairing interaction operator $\hat{H}_P$ is shown as a function of the temperature T. While the system with $G=20$ MeV/56 reaches full pairing strength at temperatures $T\leqslant 0.4$ MeV, the system with $G=10$ MeV/56 comes to this regime only at values of $T\leqslant 0.2$ MeV. In Fig. 9 the number of particles in the $1f_{7/2}$ orbital and the number of particles in the other orbitals are shown. For the system with $G=10$ MeV/56, it is observed that approximately all six particles occupy states in the $1f_{7/2}$ orbital for values of $T\leqslant 0.45$ MeV. The fact that the pairing correlations reach their maximum for this system only at values of $T\leqslant 0.2$ MeV means that the system passes through two

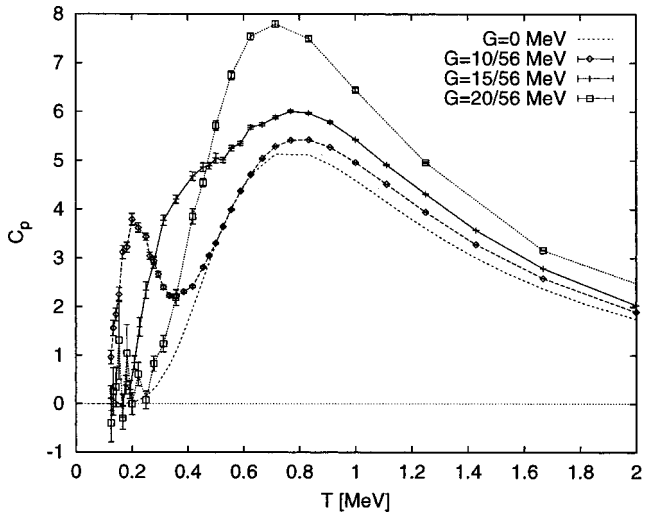

FIG. 7. Proton specific heat C_p as a function of temperature T for 6 protons in the $1f_{7/2}2p_{3/2}2p_{1/2}1f_{5/2}$ shell for various values of the pairing strength G.

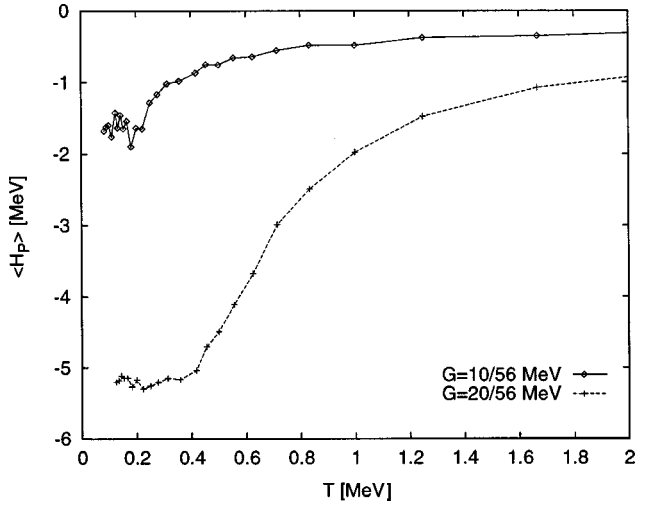

FIG. 8. Expectation value of the pairing-interaction operator $\langle \hat{H}_2 \rangle$ as a function of temperature T for pairing strength $G=10$ MeV/56 and $G=20$ MeV/56 and 6 protons in the $1f_{7/2}2p_{3/2}2p_{1/2}1f_{5/2}$ shell. No error limits were determined.

phases as it is cooled: First, the six valence protons condense into the $1f_{7/2}$ orbital. At $T\simeq 0.45$ MeV, this stage is completed. If the temperature is lowered further, pair correlations among these particles can develop. At values of $T\leqslant 0.2$ MeV the system is almost completely cooled to its ground state. For the system with $G=20$ MeV/56, the occupation of the $1f_{7/2}$ orbital reaches a maximum of about 5.3. The particles always remain spread over all the valence orbitals because now the pairing interaction is strong enough to scatter them out of the $1f_{7/2}$ orbital, even in the ground state.

C. Dependence on the size of the model space

For the description of the high-temperature properties of the system, the model space given by the fp shell is too small. At temperatures of a few MeV, valence particles can be excited to higher-lying single-particle states or core par-

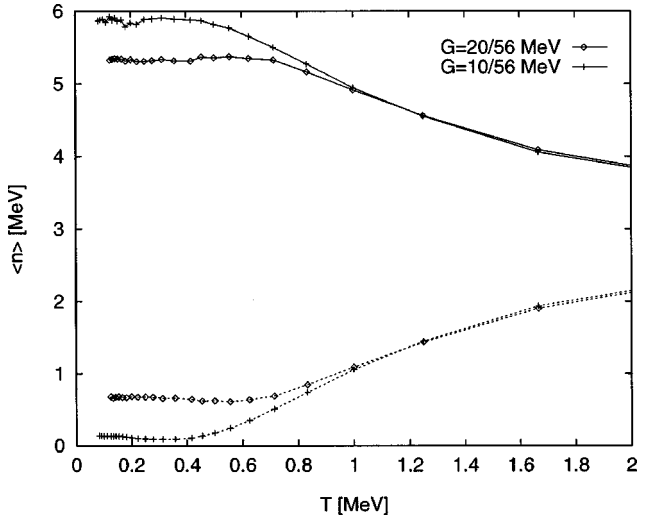

FIG. 9. Number particles in the $1f\frac{7}{2}$ orbital (full line) and in the other orbitals (dotted line) as a function of the inverse temperature β for 6 protons in the $1f_{7/2}2p_{3/2}2p_{1/2}1f_{5/2}$ shell. No error limits were determined.

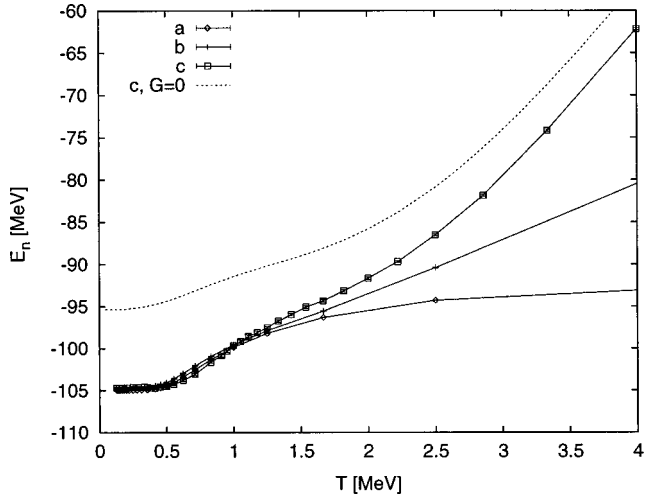

FIG. 10. Neutron energy E_n as a function of temperature T for 10 neutrons in the $1f_{7/2}2p_{3/2}2p_{1/2}1f_{5/2}$ shell (curve a), for 10 neutrons in the first extended model space (curve b) and for 30 neutrons in the second extended model space (curve c). The dashed line gives the result for the second extended model space without pairing ($G=0$). The results for the largest model space are shifted such that curves *b* and *c* coincide at low temperature.

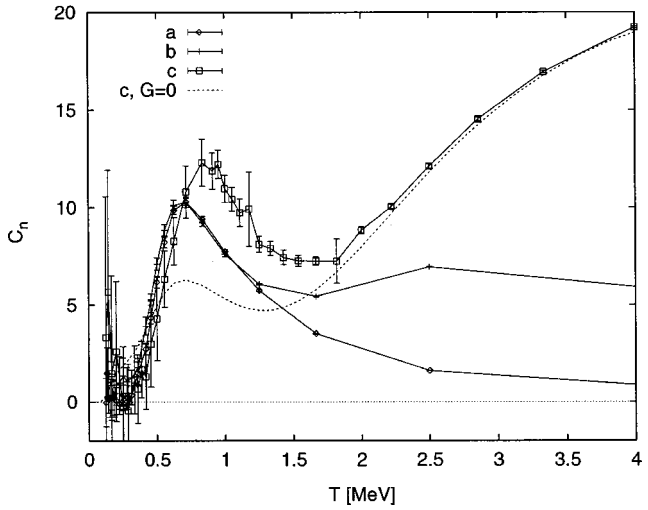

FIG. 11. Neutron specific heat C_n as a function of temperature T for 10 neutrons in the $1f_{7/2}2p_{3/2}2p_{1/2}1f_{5/2}$ shell (curve a), for 10 neutrons in the first extended model space (curve b), and for 30 neutrons in the second extended model space (curve c). The dashed line gives the result for the second extended model without pairing ($G=0$).

ticles can be excited into the valence orbitals or higher-energy states. In order to know up to what temperatures the results that we obtained in the fp shell are valid, we performed a number of calculations in larger model spaces. First, the $3s_{1/2}$, $2d_{5/2}$, $2d_{3/2}$, and $1g_{9/2}$ orbitals are added to the single-particle space. This leads to a many-body problem of 6 and 10 particles in 42 single-particle states. In a second extended model the core states are considered as valence states too. Therefore the $1s_{1/2}$, $1p_{3/2}$, $1p_{1/2}$, $1d_{5/2}$, $1d_{3/2}$, and $2s_{1/2}$ orbitals are added. Furthermore, also the $3p_{3/2}$, $3p_{1/2}$, $4s_{1/2}$, and $1g_{7/2}$ orbitals are taken into account. This leads to a many-body problem of 26 and 30 particles in 78 single-particle states.

Because multiple shells are used, the model space of the extended systems contains spurious excitations related to center-of-mass motion. Therefore, care has to be taken when relating high-temperature results to internal excitations of the system. For the largest model space (without core), these center-of-mass motions can be interpreted as thermal excitations of the collective degrees of freedom. This picture would be physically meaningful in the absence of a mean-field potential. The fact that the mean-field potential is localized in space breaks the translational invariance of the model. Therefore, one cannot separate the center-of-mass motion from the intrinsic excitations in a clean way [25]. A consistent treatment of spurious states is a topic for further research.

The results for the energy and the specific heat obtained using these model spaces are shown in Figs. 10–13. If the value for the pairing interaction strength G is not changed, then a system with a larger model space will have a lower ground-state energy because the larger model space allows stronger pair correlations. In order to obtain a comparable pairing energy, a reduced pairing interaction strength of $G=16$ MeV/56 is used for the extended model spaces. For the no-core system, the energy is shifted such that the ground-state energy coincides with the ground-state energy of the fp shell system.

In the largest model space, at high temperatures ($T \geqslant 2$ MeV), the specific-heat curve coincides with the specific-heat curve for $G=0$. In this temperature region, the proton and neutron energy are some 5 MeV lower than in the $G=0$ case. Apart from this shift, the energy curves are similar to the $G=0$ case. This indicates that, at high temperatures, the pairing Hamiltonian enhances the binding energy but has no effect on the internal structure.

At lower temperatures, the specific-heat curve deviates from the curve for $G=0$ because pairing correlations de-

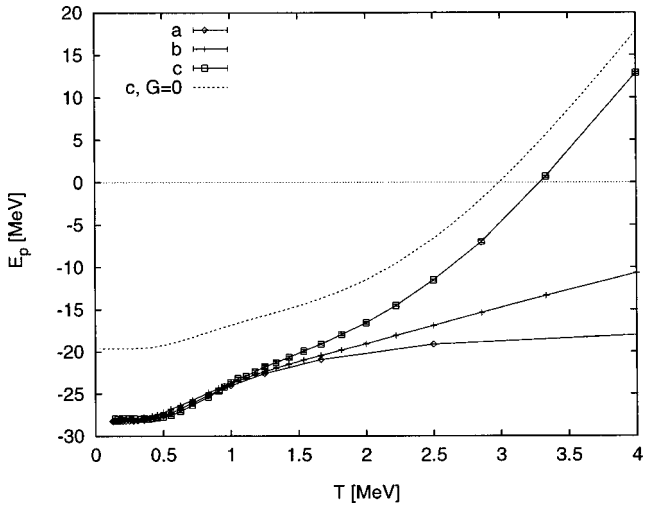

FIG. 12. Proton energy E_p as a function of temperature T for 6 protons in the $1f_{7/2}2p_{3/2}2p_{1/2}1f_{5/2}$ shell (curve a), for 6 protons in the first extended model space (curve b), and for 26 protons in the second extended model space (curve c). The dashed line gives the result for the second extended model without pairing ($G=0$). The results for the largest model space are shifted such that curves *b* and *c* coincide at low temperature.

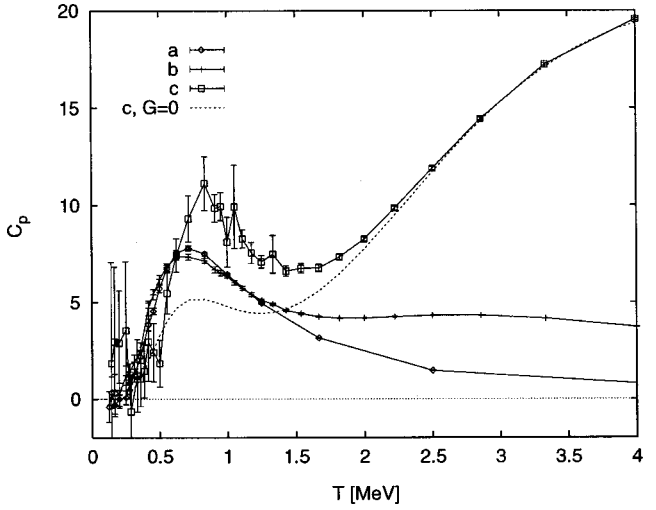

FIG. 13. Proton specific heat C_p as a function of temperature T for 6 protons in the $1f_{7/2}2p_{3/2}2p_{1/2}1f_{5/2}$ shell (curve a), for 6 protons in the first extended model space (curve b), and for 26 protons in the second extended model space (curve c). The dashed line gives the result for the second extended model without pairing ($G=0$).

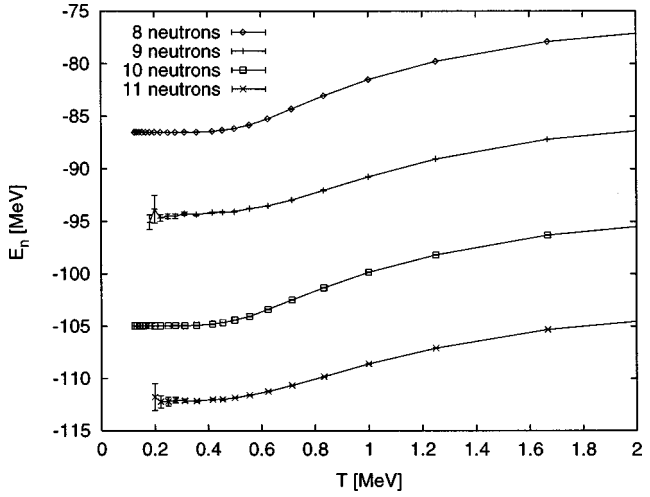

FIG. 14. Neutron energy E_n as a function of temperature T for systems with 8, 9, 10, and 11 neutrons in the $1f_{7/2}2p_{3/2}2p_{1/2}1f_{5/2}$ shell ($G=20$ MeV/56).

velop. By comparing the results for the fp shell and the first extended model space, we see that even the fp shell is too small to describe the system at temperatures $T \geqslant 1.3$ MeV. In order to compare with the results for the second extended model space around temperatures of 1 MeV, the pairing interaction strength G ought to be reduced somewhat more for the latter model space. The vanishing of pair correlations with increasing temperature, starting from $T \simeq 1$ MeV, was also observed in shell-model quantum Monte Carlo calculations for $^{54}_{26}\mathrm{Fe}_{28}$ based on more realistic interactions [3,4]. The interesting topic of proton-neutron pairing in $N=Z$ nuclei [26] could not be addressed of course in our too schematic model used at present.

The schematic form of the interaction has a caveat: In the larger model spaces, the pairing interaction scatters particles into Woods-Saxon orbitals that extend into regions where the mean field vanishes (the orbitals beyond the core and the fp shell). Because the pairing interaction introduces correlations in the angular coordinates but not in the radial coordinates, one might expect the ground-state wave function to extend too far into space. A more realistic interaction would localize the wave function more closely to the core. Our calculations show that these extended orbitals contribute only about 1% of the ground-state density. Therefore, we think that this has only a minor effect on the energylike observables we are interested in here.

D. Dependence on the number of particles

We studied systems with various numbers of neutrons in the fp shell: $^{54}_{26}\mathrm{Fe}_{28}$, $^{55}_{26}\mathrm{Fe}_{29}$, $^{56}_{26}\mathrm{Fe}_{30}$, and $^{57}_{26}\mathrm{Fe}_{31}$ are modeled by considering eight, nine, ten, and eleven neutrons in the fp valence shell, respectively. For the systems with 9 and 11 neutrons, the sign problem limits accurate calculations to values of $T \geqslant 0.25$ MeV. Fortunately, this temperature is low enough to get a good approximation of the ground state. The neutron energy E_n for the various systems is shown as a function of temperature in Fig. 14. The proton internal energy is not shown because it is equal for all four systems and it is already given in Fig. 6. While at high temperature the energy curves are equidistantly spaced, with an interval of about 9 MeV, there is a relative shift to lower energies for the systems with eight and ten neutrons at low energy. This is because the pairing correlations are stronger for the even systems than for the odd systems at temperatures below 1 MeV. The shift in the energy for the system with ten neutrons can be quantified as

$$\Delta E_{10} = \frac{E_{n9} + E_{n11}}{2} - E_{n10}, \tag{24}$$

with E_{n9}, E_{n10}, and E_{n11} the neutron energies for the systems with nine, ten, and eleven valence neutrons, respectively. The quantity ΔE_{10} is shown as a function of temperature in Fig. 15. The ground-state energy shift was calculated analogously to expression (24), with the energies replaced by the mass excesses given in Ref. [27]. A value of 1.776 MeV

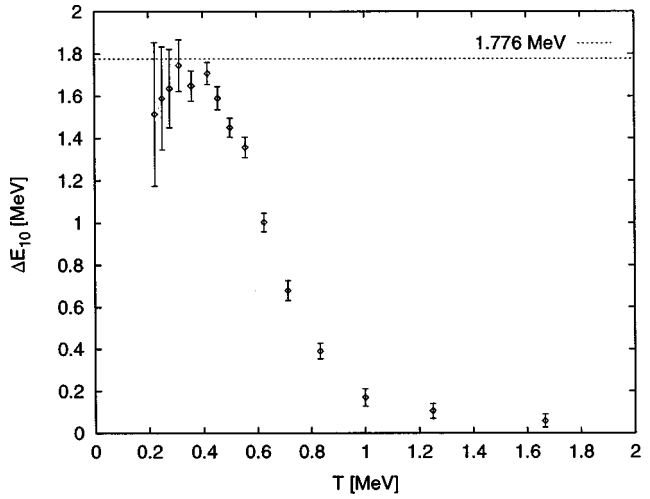

FIG. 15. Neutron energy shift ΔE_{10} as a function of temperature T for systems with 10 neutrons in the $1f_{7/2}2p_{3/2}2p_{1/2}1f_{5/2}$ shell ($G=20$ MeV/56). The dashed line indicates the experimental value of the ground-state energy shift for $^{56}_{26}\mathrm{Fe}_{30}$.

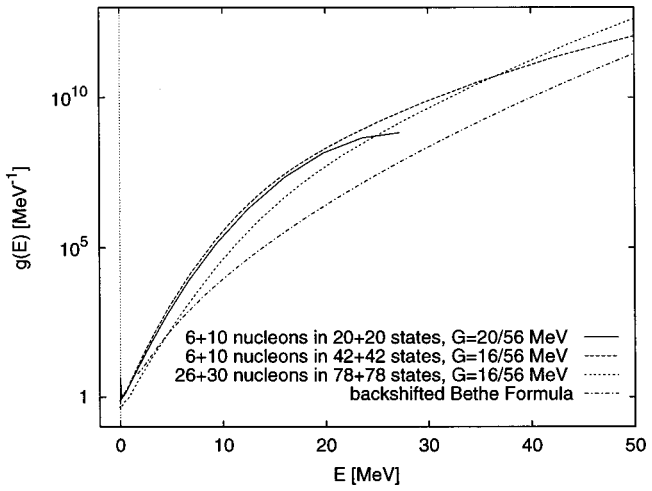

FIG. 16. Level densities for several model spaces. The ground-state energy in each model space was shifted to 0 MeV. The backshifted Bethe formula was fitted to experimental data for ^{56}Fe (for temperatures up to 10^{10} K).

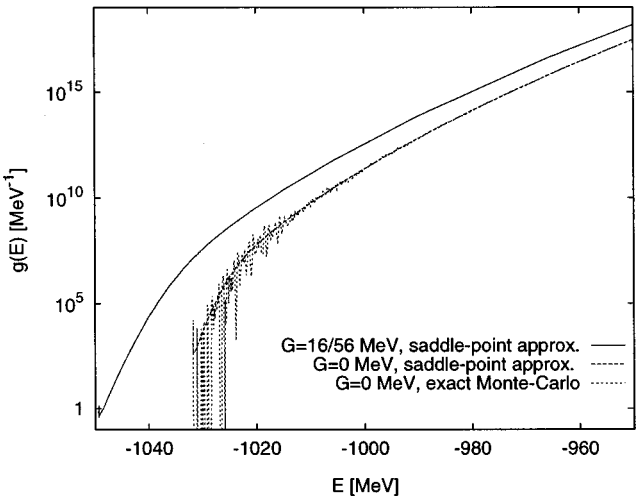

FIG. 17. Level densities for the largest model space, with and without the pairing interaction. The energy scale reflects the sum of the single-particle energies as listed in Table I and the additional binding energy stemming from the pairing interaction.

is obtained. Our quantum Monte Carlo results approach this value remarkably well at temperatures below 0.5 MeV.

E. Level densities

Because the internal energy is related to the derivative of the logarithm of the partition function Z_β and because Z_β is the Laplace transform of the level density $g(E)$ of excited states, the results presented above also give information about the level density. The partition function can be obtained by numerical integration of the internal energy. Then one should apply an inverse Laplace transform on Z_β. Because of the statistical errors on the internal energies and hence on Z_β, this is, however, an ill-posed problem. A good approximation (at high enough energies) is given by the saddle-point approximation

$$g(E)=\frac{e^{\beta E}Z_\beta}{\sqrt{2\pi(\beta^{-2}C)}}. \tag{25}$$

Our quantum Monte Carlo method gives accurate results for E and $\beta^{-2}C$. So the level density in the saddle-point approximation is easily obtained. Figure 16 shows the level densities derived from the results shown in Figs. 10–13. The results for the smallest model space only go up to excitation energies of 25 MeV. They are in good agreement with the results for the first extended model space, up to energies of 20 MeV. However, the results for the largest model space deviate from these, even at energies below 20 MeV. This indicates that it is important to consider also core excitations when calculating level densities. Figure 16 also shows the level-density curve from a backshifted Bethe formula cited in reference [6], with parameters $a=5.80$ MeV^{-1} and $\Delta=1.38$ MeV. This parametrization was fitted to experimental data [28] in order to reflect finite-temperature properties at temperatures between 10^7 and 10^{10} K. Clearly, the level densities are shifted too much to lower energies by the residual interaction we considered. Shell-model Monte Carlo calculations with a more realistic interaction, but in a limited model space (the $1f_{7/2}2p_{3/2}2p_{1/2}1f_{5/2}1g_{9/2}$ shell), result in a better agreement with the backshifted Bethe formula at energies between 5 and 20 MeV [6].

Figure 17 compares the level density for the largest model space with the level density for the mean-field Hamiltonian. For the mean-field case, the level density can be calculated exactly using a Monte Carlo method devised by Cerf [29]. We performed such a calculation for the largest model space in order to compare it with the saddle-point approximation. For this largest model space, the saddle-point results follow closely the exact level density at high energies. At lower energies, the exact level density shows a structure with many peaks because of the discrete structure of the spectrum. In the saddle-point approximations these peaks are absent. If these peaks are smeared out with a width of 0.5 MeV, the curve coincides with the saddle-point approximation even at excitation energies as low as 1 MeV. Thus the saddle-point approximation gives a good ''smoothed'' estimate. In the smaller model spaces the agreement is less good. Figure 17 shows that the residual interaction shifts level densities to lower energies. This shift is largest at low energies because there the pairing correlations are strongest.

V. CONCLUSION

We conclude by stating that our quantum Monte Carlo method offers a powerful tool for the study of the nuclear pairing model. We have put emphasis on the thermodynamical properties. Occupation numbers and the pairing gap can be calculated too using this method. Main advantages over other methods are that many-body correlations are taken into account exactly, particle numbers are constant, and finite temperature results can be obtained. The major disadvantage of the method is that spectroscopic information can be obtained only indirectly. Finally, we remark that our calculations indicate that pairing correlations are important only at low temperature (below 1 MeV) and at low excitation energies, though they do enhance the binding energy. A signal of

a phase transition related to pairing is found at temperatures around 0.7 MeV. The pairing interaction also shifts the level density towards lower energies. Furthermore, our results show that it is necessary to work in very large model spaces, which also include core excitations, if one wants to calculate accurate level densities. The work presented here constitutes a part of [30].

ACKNOWLEDGMENTS

Discussions with K. Langanke, C.W. Johnson, W.E. Ormand, and S. Goriely are gratefully acknowledged. The authors are grateful to the FWO (Fund for Scientific Research) Flanders and to the Research Board of the University of Gent for financial support. One of the authors (K.H.) is grateful to CERN for financial support.

[1] B. S. Pudliner, V. R. Pandharipande, J. Carlson, and R. B. Wiringa, Phys. Rev. Lett. **74**, 4396 (1995).
[2] S. E. Koonin, D. J. Dean, and K. Langanke, Phys. Rep. **278**, 1 (1997).
[3] D. J. Dean, S. E. Koonin, K. Langanke, P. B. Radha, and Y. Alhassid, Phys. Rev. Lett. **74**, 2909 (1995).
[4] K. Langanke, D. J. Dean, p. B. Radha, and S. E. Koonin, Nucl. Phys. **A602**, 244 (1996).
[5] W. E. Ormand, Phys. Rev. C **56**, 1678 (1997).
[6] H. Nakada and Y. Alhassid, Phys. Rev. Lett. **79**, 2939 (1997).
[7] P. Ring and P. Schuck, *The Nuclear Many-Body Problem* (Springer, New York, 1980), p. 217.
[8] R. W. Richardson and N. Sherman, Nucl. Phys. **52**, 221 (1964).
[9] O. Burglin and N. Rowley, Nucl. Phys. **A602**, 21 (1996); **A609**, 600(E) (1996).
[10] N. J. Cerf and O. Martin, Phys. Rev. C **47**, 2610 (1993).
[11] R. D. Woods and D. S. Saxon, Phys. Rev. **95**, 577 (1954).
[12] C. M. Perey and F. G. Perey, Nucl. Data Tables **10**, 540 (1972).
[13] D. R. Bes and R. A. Sorensen, Adv. Nucl. Phys. **2**, 129 (1969).
[14] N. Metropolis, A. W. Rosenbluth, M. N. Rosenbluth, A. H. Teller, and E. Teller, J. Chem. Phys. **21**, 1087 (1953).
[15] M. Suzuki, Phys. Lett. A **146**, 319 (1991).
[16] S. Rombouts, K. Heyde, and N. Jachowicz, Phys. Lett. A **242**, 271 (1998).
[17] J. Hubbard, Phys. Rev. Lett. **3**, 77 (1959).
[18] R. D. Stratonovich, Dokl. Akad. Nauk. SSSR **115**, 1907 (1957) [Sov. Phys. Dokl. **2**, 416 (1958)].
[19] S. Rombouts and K. Heyde, J. Comput. Phys. **140**, 453 (1998).
[20] W. E. Ormand, D. J. Dean, C. W. Johnson, G. H. Lang, and S. E. Koonin, Phys. Rev. C **49**, 1422 (1994).
[21] S. Fahy and D. R. Hamann, Phys. Rev. B **43**, 765 (1991).
[22] W. von der Linden, Phys. Rep. **220**, 53 (1992).
[23] Y. Alhassid, D. J. Dean, S. E. Koonin, G. H. Lang, and W. E. Ormand, Phys. Rev. Lett. **72**, 613 (1994).
[24] W. K. Hastings, Biometrika **57**, 97 (1970).
[25] R. D. Lawson, *Theory of the Nuclear Shell Model* (Clarendon, Oxford, 1980), p. 223.
[26] K. Langanke, D. J. Dean, S. E. Koonin, and P. B. Radha, Nucl. Phys. **A613**, 253 (1997).
[27] J. K. Tuli, *Nuclear Wallet Cards* (The U.S. Nuclear Data Network, Brookhaven National Laboratory, Upton, NY, 1995).
[28] S. E. Woosley, W. A. Fowler, J. A. Holmes, and B. A. Zimmerman, At. Data Nucl. Data Tables **22**, 371 (1978).
[29] N. J. Cerf, Phys. Lett. B **268**, 317 (1991).
[30] S. Rombouts, Ph.D. thesis, University of Ghent, 1997.